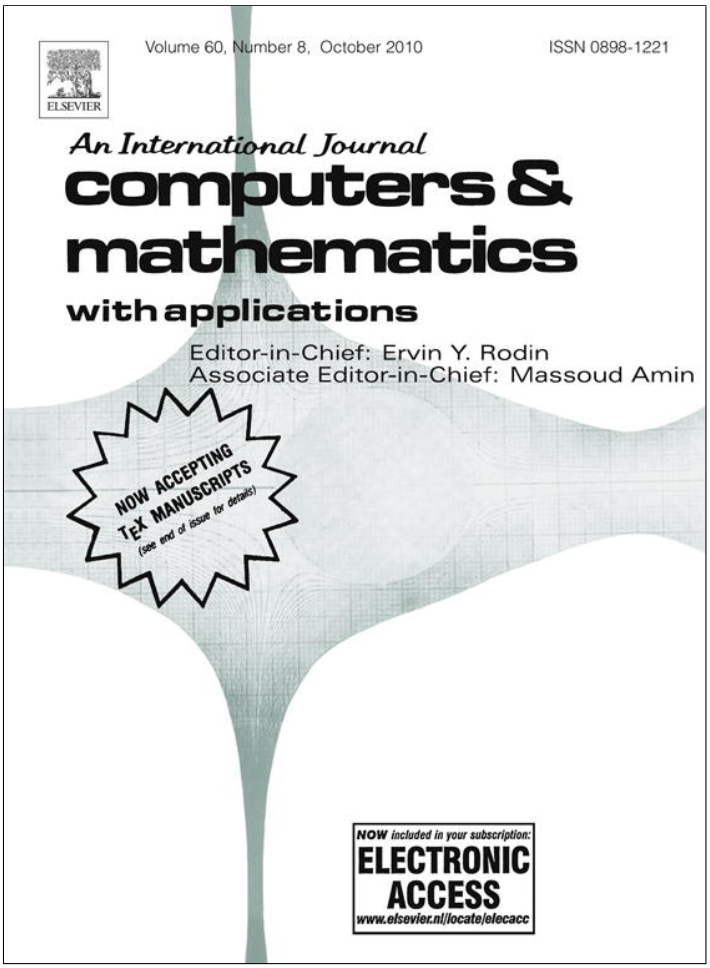

Computers and Mathematics with Applications 60 (2010) 2239–2252

Contents lists available at ScienceDirect

Computers and Mathematics with Applications

journal homepage: www.elsevier.com/locate/camwa

Moving mesh partial differential equations to describe nematic order dynamics

A. Amoddeo [a], R. Barberi [b], G. Lombardo [b,*]

[a] Mechanics and Materials Department, University "Mediterranea" of Reggio Calabria, Via Graziella 1, Feo di Vito, 89122 Reggio Calabria, Italy
[b] CNR IPCF LiCryL – Liquid Crystal Lab., Physics Department, University of Calabria, via P. Bucci, Cubo 32/c, 87036 Arcavacata di Rende (CS), Italy

ARTICLE INFO

Article history:
Received 13 October 2009
Received in revised form 17 May 2010
Accepted 6 August 2010

Keywords:
Nematic liquid crystals
Order reconstruction
Biaxiality
MMPDE
FEM

ABSTRACT

Nematic liquid crystals are aggregates of calamitic molecules and most related experimental phenomena are described well by their mean molecular orientation, i.e. by the director, and by the scalar order parameter, considering a perfect uniaxial symmetry. However, when the nematic distortion is very strong and it occurs over a length scale comparable with the nematic coherence length, the molecular order may be significantly altered, as in the case of the core of a defect or in the case of highly frustrated nematic systems. Such systems, where spatial and/or temporal changes of the nematic order are relevant, require a full Landau-de Gennes **Q**-tensor description.

In this work, we will present the implementation of a **Q**-tensor numerical model, based on a one-dimensional finite element method with a r-type moving mesh technique capable of describing the nematic order dynamics inside a π-cell submitted to a strong electric pulse. The use of the moving grid technique ensures no waste of computational effort in the area of low spatial order variability: in fact, the technique concentrates the grid points in regions of large $\nabla\mathbf{Q}$, maintaining constant the total number of nodes in the domain.

1. Introduction

Nematic liquid crystals are aggregates of calamitic molecules which do not present any positional order and whose long axes are directed along a common direction, the director **n**, along which the degree of orientation is described by the scalar order parameter S. Classically the nematic phase is described by the Frank–Oseen theory [1–3] where usually **n** can vary and S is considered practically constant everywhere. This theory is able to correctly describe elastic problems, i.e. the application of an external field (electric, magnetic or mechanic) inducing elastic stress to the fundamental state of the nematic molecules allowing the orientation of **n** to vary in space. This is the case, for instance, of monostable transitions, as the well known Freedericks transition, where a starting texture, prescribed by suitable boundary conditions, is elastically distorted by an external electric or magnetic field. In these systems, the distortion always relaxes back to its initial equilibrium configuration when the external perturbation is removed. Monostable electro-optical transitions are today used to control the behaviour of the well known nematic liquid crystal displays, which are in fact monostable devices. However, there exist situations in which experimental results cannot be fully described by this classical approach. When the nematic distortion is very strong and it occurs over a length scale comparable with the nematic coherence length [4], the minimum distance over which the nematic molecules are on average aligned along **n**, the molecular order may be significantly altered, as in the case of the core of a defect [5]. Moreover the standard simplified elastic theory fails also for recent experimental results on phase

* Corresponding author. Tel.: +39 0984 496150; fax: +39 0984 494401.
E-mail addresses: antonino.amoddeo@unirc.it (A. Amoddeo), barberi@fis.unical.it (R. Barberi), lombardo@fis.unical.it, giuseppe.lombardo@cnr.it (G. Lombardo).

0898-1221/$ – see front matter © 2010 Elsevier Ltd. All rights reserved.
doi:10.1016/j.camwa.2010.08.014

transitions induced by nano-confinement [6] and for the electric field induced order reconstruction [7–12]. Such systems, where spatial and temporal changes of the nematic order are relevant and biaxial transient nematic configurations arise, require a full Landau-de Gennes **Q**-tensor description [13].

The creation of transient biaxial states inside a nematic material allows transitions between textures with different topologies, which are forbidden in the Frank–Oseen model [14]. For example, this is the case of a π-cell submitted to an high electric field, in which an initial splay texture is transformed into a topological different bend texture by means of the electric field induced nematic order reconstruction [7–12]. This phenomenon allows connecting two different topological nematic textures, changing the local molecular order of the phase without any macroscopic director rotation. The dynamical evolution is then described by means of the order tensor **Q** where the eigenvectors are the preferred molecular orientation and the associated eigenvalues measure the degree of order [15].

The order reconstruction phenomenon takes place whenever two conflicting uniaxial states are recomposed in space through a variety of transient biaxial states [7]. Typically, the biaxial order decays in space with a characteristic length of about ten nanometers and, being the scale of usual physical problems in the order of some micrometers, sophisticated numerical modelling techniques are required in order to obtain reliable results, since molecular dynamics [16] and Monte Carlo simulations [17,18] are in agreement with the prediction of Landau-de Gennes theory for confined liquid crystals films.

In this direction, the Finite Element Method (FEM), used for application in several research branches, provides computational mathematics with a powerful tool to solve Partial Differential Equation (PDE) systems arising from problem modelling [19,20]. In one-dimensional studies of a nematic liquid crystal confined in a cell, we look for the nematic texture that minimises the energy functional of the problem [1]. The integration domain is divided in elements composed by nodes on which the solution is found and the spatial variation of **Q** inside each element is interpolated by suitable shape functions. Discretisation of the integration domain into an appropriate grid of points is very crucial, particularly in frustrated nematic systems where the gradient of the order and the local and transient biaxiality become important. Adaptive grid techniques can be used to solve these phenomena, ensuring no waste of computational effort in areas where there is no need for finer grids. In the literature, two main methods are described in order to tackle the problem: static (*h*-type, *p*-type) or dynamic (*r*-type) remeshing methods. The former (*h*-type) are based on the insertion of extra mesh points to satisfy tolerance requirements, but this can result in an undesired huge amount of points, is very memory and time consuming, unpractical to store and manage; on the other hand, *p*-type remeshing techniques keep constant the element size increasing the order of the polynomial used to represent the solution within each element, as smoothness permits. The latter method, instead, keeps constant nodal connectivity and the number of mesh points inside the domain: simply, mesh points are moved towards regions where more detail is required [21].

Several efforts have been done recently to model liquid crystal systems by FEM. Barrett et al. [22], consider a degenerate parabolic system which models the evolution of nematic liquid crystals with variable degree of orientation, proposing a fully discrete FEM approximation for the regularised system. Patricio et al. [23], studying the colloidal dipolar interactions in 2D smectic-C films, use FEM with adaptive meshing to minimise the 2D elastic free energy. James et al. [24] developed a FEM model of a nematic liquid crystal hydrodynamics in order to allow a proper description of disclinations. They all use static remeshing techniques [21]. See also Ref. [25] for an overview on previous literature. Recently, two of us applied *h*-type static remeshing methods to solve a FEM model inside nematic liquid crystal systems [10–12], while Ramage and Newton [25] used a dynamical remeshing method to reproduce numerical results obtained in Ref. [7]. In this case, due to the geometry of the considered domain, confining layers of the liquid crystal become enriched with grid points, starving the bulk region. Moreover, this approach is subject to arbitrary parametric choices in order to tune the overall adaptivity.

In this work we present a novel implementation of the Moving Mesh Partial Differential Equations (MMPDE) numerical technique applied to an improved model, capable of describing the overall dynamical transition inside a π-cell submitted to an electric field [12]. Throughout the paper, we will refer to anchoring as the effect of the interaction of a liquid crystal molecule with a confining surface, resulting in a molecule's orientation along a given direction. The numerical calculations are performed using an adaptive *r*-type algorithm, improved with respect to that presented in Ref. [25], in order to cluster greater amounts of grid points outside confining layers and reducing external intervention. The use of the moving grid technique ensures no waste of computational effort in the area of low spatial order variability: in fact, the technique concentrates the grid points in regions of large $\nabla\mathbf{Q}$ maintaining constant the total number of the nodes in the domain.

2. Q tensor nematic description

Modelling the **Q**-tensor response of a nematic to an external field goes through a minimisation of the free energy density functional inside the cell containing the liquid crystal, where the main contributions come from thermotropic, elastic and electric terms. In the Landau-de Gennes framework the free energy density F is expressed in powers of **Q**, assuming its dependence from small **Q** distortions. For a complete review see, for example, Refs. [1,15].

A nematic liquid crystal texture is globally described by the symmetric, second-rank, traceless tensor in the orthonormal basis of its eigenvectors $\{\mathbf{e}_1, \mathbf{e}_2, \mathbf{e}_3\}$

$$\mathbf{Q} = \sum_{i=1}^{3} \lambda_i \mathbf{e}_i \otimes \mathbf{e}_i \tag{1}$$

where λ_i are the eigenvalues of **Q** corresponding to the eigenvectors $\mathbf{e}_i$, thus obeying the condition $\lambda_1 + \lambda_2 + \lambda_3 = 0$.

In fact, let the symmetric, second order $\mathbf{M}$ and $\mathbf{M}_0$ tensors be associated with, respectively, a given and an isotropic probability distribution [15], the order tensor $\mathbf{Q}$ is defined as $\mathbf{Q} = \mathbf{M} - \mathbf{M}_0$, and gives a measure of how the second moments tensor $\mathbf{M}$ deviates from $\mathbf{M}_0$ [1]. Since from statistical considerations, $\operatorname{tr}\mathbf{M} = 1$ and $\operatorname{tr}\mathbf{M}_0 = (1/3)\mathbf{I}$, with $\mathbf{I}$ the identical tensor, it follows that $\operatorname{tr}\mathbf{Q} = 0$.

In this respect, describing a nematic molecules arrangement, only five independent parameters are necessary, i.e. five lagrangian parameters q_i, $i \in [1,5]$, corresponding to the five degrees of freedom of a rod-shaped nematic molecule:

$$\mathbf{Q} = \begin{pmatrix} q_1 & q_2 & q_3 \\ q_2 & q_4 & q_5 \\ q_3 & q_5 & -q_1 - q_4 \end{pmatrix}. \tag{2}$$

We are interested in a description of nematics in biaxial configurations, so a complete representation of (1), or (2), has to be used, since $\mathbf{Q}$ is a tensor field varying inside our domain.

In order to measure the degree of biaxiality, we use the definition used in Ref. [7]

$$\beta^2 = 1 - 6\frac{\operatorname{tr}(\mathbf{Q}^3)^{\,2}}{\operatorname{tr}(\mathbf{Q}^2)^3} \in [0, 1] \tag{3}$$

which is an invariant measure of the biaxiality. The eigenvectors $\mathbf{e}_1$, $\mathbf{e}_2$, and $\mathbf{e}_3$ of $\mathbf{Q}$ are the directions of the preferred molecular orientations and the associated eigenvalues λ_1, λ_2, and λ_3 represent the degree of order along each corresponding direction. Calamitic nematic materials can present three different phases (isotropic, uniaxial and biaxial) which can be distinguished considering λ_1, λ_2, and λ_3. In the isotropic phase the calamitic molecules are completely disordered, without any positional and orientational order, and all the three eigenvalues vanish. In this phase, the optical behaviour of the material is as an ordinary isotropic fluid. The uniaxial nematic phase presents a unique optical axis, described by the eigenvector $\mathbf{e}_i = \mathbf{n}$ associated to the maximum eigenvalue $\lambda_{\max}$, which gives the scalar order parameter $S = (3/2)\lambda_{\max}$. In the biaxial nematic phase, all the eigenvalues are different, the Fresnel ellipsoid has two optical axes and the maximum of biaxiality is attained when at least one eigenvalue vanishes, see Eq. (3), since $\operatorname{tr}\mathbf{Q}^3 = 3\det\mathbf{Q}$ vanishes too. When $\beta^2 = 0$ then the nematic texture is uniaxial; instead, the maximum of biaxiality corresponds to $\beta^2 = 1$, when the nematic phase is biaxial.

Brimicombe and Raynes [26] demonstrated both experimentally and theoretically that nematic liquid crystals confined in a π-cell in a splay symmetric configuration do not experience backflow during switching to a vertical configuration, due to the symmetry of both states. As a consequence, the dynamical evolution of the system is given by solutions of a PDE equation system of the type

$$\frac{\partial D}{\partial \dot{q}_i} + \frac{\partial F_t}{\partial q_i} + \frac{\partial F_e}{\partial q_i} + \frac{\partial F_d}{\partial q_i} - \frac{\partial}{\partial x_j}\left(\frac{\partial F_d}{\partial q_{i,j}}\right) - \frac{\partial}{\partial x_j}\left(\frac{\partial F_e}{\partial q_{i,j}}\right) = 0 \quad i = 1\ldots 5 \tag{4}$$

with suitable boundary conditions, obtained from a generalized Euler-Lagrange equation. In (4) we assume summation over repeated indices, and the subscript "j" denotes differentiation with respect to the spatial coordinate $\mathbf{x}_j$. Here D is the dissipation function giving rise to a generalized force term; F_t, F_e and F_d are, respectively, thermotropic, electric and elastic energy densities. Considering infinite anchoring strength, and therefore Dirichlet boundary conditions for the liquid crystal, the surface contribution to the energy density is neglected since the boundary conditions are fixed, and the above equations come out assuming that

$$F_t = F_t(\mathbf{Q}), \qquad F_e = F_e(\mathbf{Q}, \nabla\mathbf{Q}), \qquad F_d = F_d(\mathbf{Q}, \nabla\mathbf{Q}). \tag{5}$$

In detail

$$F_t = a\operatorname{tr}(\mathbf{Q}^2) - \frac{2b}{3}\operatorname{tr}(\mathbf{Q}^3) + \frac{c}{2}(\operatorname{tr}(\mathbf{Q}^2))^2 \tag{6}$$

with $a = \alpha(\mathrm{T} - \mathrm{T}^*) = \alpha\Delta\mathrm{T}$, $\alpha > 0$ and b and c are temperature dependent, but often approximated as constants. Here T^* is the super-cooling temperature [27] at which the isotropic state of the liquid crystal becomes unstable.

$$F_e = -\frac{\varepsilon_0}{2}\left(\varepsilon_i\,|\nabla U|^2 + \varepsilon_a \nabla U \cdot \mathbf{Q}\nabla U\right) + \bar{e}\nabla\mathbf{Q}\cdot\nabla U \tag{7}$$

with

$$\bar{e} = \frac{e_{11} + e_{33}}{2S_{\mathrm{eq}}} \tag{8}$$

where e_{11} and e_{33} are the splay and bend flexoelectric coefficients, ε_i and ε_a are the isotropic and the anisotropic dielectric susceptibilities, U is the electric potential, while

$$S_{\mathrm{eq}}\,(\Delta T) = \frac{b}{4c}\left(1 + \sqrt{1 - \frac{24ac}{b^2}}\right) \tag{9}$$

is the equilibrium order parameter for uniaxial systems.

$$F_d = \frac{L_1}{2}\left(\frac{\partial Q_{ij}}{\partial x_k}\right)^2 + \frac{L_2}{2}\frac{\partial Q_{ij}}{\partial x_j}\frac{\partial Q_{ik}}{\partial x_k} + \frac{L_6}{2}Q_{lk}\frac{\partial Q_{ij}}{\partial x_l}\frac{\partial Q_{ij}}{\partial x_k} \tag{10}$$

with

$$\begin{aligned} L_1 &= \frac{1}{6S_{\text{eq}}^2}(k_{33} - k_{11} + 3k_{22}) \\ L_2 &= \frac{1}{S_{\text{eq}}^2}(k_{11} - k_{22}) \\ L_6 &= \frac{1}{2S_{\text{eq}}^3}(k_{33} - k_{11}) \end{aligned} \tag{11}$$

and k_{11}, k_{22} and k_{33} the Frank elastic constants.

Beside Eq. (4), we need the governing equation for the electric potential

$$\nabla \cdot D = \nabla \cdot (-\varepsilon_0 \varepsilon \nabla U + P_S) = 0 \tag{12}$$

where $\mathbf{D}$ and ε_0 are, respectively, the displacement field and the vacuum dielectric permeability; the dielectric tensor is expressed as [15] $\varepsilon = \varepsilon_a \mathbf{Q} + \varepsilon_i \mathbf{I}$, and the spontaneous polarisation vector, ensuring that, in the static case, the electric field inside the cell obeys Maxwell equations for conservative field and in absence of source charges, is expressed as [28] $P_S = \bar{e}\nabla\mathbf{Q}$.

3. The adaptive moving mesh method

As stated above, r-type remeshing method comes from a class of dynamic refinement techniques in which the mesh points are concentrated in regions of high spatial variability and at the same time they are pulled away from regions of low activity, keeping their number always constant.

The common idea of such moving methods is to find an *appropriate* mesh map capable of capturing each significant solution feature. This is achieved defining a monitor function, a quality functional as solution evolves in time. For one-dimensional problems, a commonly used technique is based on the *equidistribution principle* [29,30], in which the mesh map quality is controlled by equidistributing in each subinterval the monitor function, which can depend, in turn, on the solution gradient of the unknown solution [25,31], or on the interpolation error [32]. This method is quite efficient, since it allows extremely accurate representations of sharp solution features, such as shocks or defects. Unfortunately it is less robust than static refinement, since the maximal possible accuracy depends on the initial number of mesh points.

Many different ways of generating adaptive meshes based on equidistribution principles have been developed. In practice, the monitor function can be based on a simple function of the derivatives of the unknown solution, and his optimal choice depends on the problem being solved, the numerical discretisation being used, and the norm of the error that is to be minimised [31]. Here we illustrate the ideas involved to define two different monitor functions, the Arch-Length (AL) and the Beckett-Mackenzie (BM) monitor functions and we apply them to solve the dynamical evolution of the order parameter tensor inside a π-cell submitted to an electric field.

If $u(z, t)$ is a solution over a physical domain $\Omega_p = [0, 1]$ of a system PDE's, z being the physical coordinate, introducing a fixed computational domain $\Omega_c = [0, 1]$ with ξ computational coordinate, a coordinate transformation is defined as

$$z = z(\xi, t), \quad \xi \in \Omega_c, t \in (0, T] \tag{13}$$

from the computational space $\Omega_c \times (0, T]$ to the physical space, $\Omega_p \times (0, T]$ and

$$\xi = \xi(z, t), \quad z \in \Omega_p, t \in (0, T] \tag{14}$$

from the physical space $\Omega_p \times (0, T]$ to the computational space $\Omega_c \times (0, T]$.

The first relation represents a one-to-one mapping at time t from computational to physical space, and a uniform grid

$$\xi_i = i/N, \quad i = 0, 1, \ldots N \tag{15}$$

imposed on computational space, corresponds to a set of nodes on physical space

$$0 = z_0(t) < z_1(t) < \cdots z_N(t) = 1. \tag{16}$$

The mesh map quality is controlled by equidistributing the monitor function $M(u(z, t))$ over the entire domain.

The one-dimensional equidistribution principle is expressed as

$$\int_0^{z(\xi,t)} M(u(s, t))\mathrm{d}s = \xi \int_0^1 M(u(s, t))\mathrm{d}s \quad i = 1 \ldots N - 1, \ \forall t \tag{17}$$

which, in discrete form becomes

$$\int_{z_i(t)}^{z_{i+1}(t)} M(u(s,t))\mathrm{d}s = \int_{z_{i-1}(t)}^{z_i(t)} M(u(s,t))\mathrm{d}s, \tag{18}$$

or

$$\int_{z_{i-1}(t)}^{z_i(t)} M(u(s,t))\mathrm{d}s = \frac{1}{N}\int_0^1 M(u(s,t))\mathrm{d}s. \tag{19}$$

The coordinate mapping $z(\xi, t)$ can be determined by differentiating (17) with respect to ξ, giving

$$M(z(x,t))\frac{\partial}{\partial\xi}z(x,t) = \int_0^1 M(u(s,t))\mathrm{d}s = C(t). \tag{20}$$

It follows that, at a given time, at a larger monitor function value corresponds a denser mesh, in order to keep the equidistribution of the monitor function constant over the integration domain.

Choosing the appropriate monitor function is fundamental for mesh quality control and final convergence of the FEM solution [25,29,31]. A common one is the AL monitor function

$$M(u(z,t)) = \sqrt{1+\alpha\left[\frac{\partial u(z,t)}{\partial z}\right]^2} \tag{21}$$

where α is a user prescribed scaling factor. His task is to cluster mesh points inside regions of steep solution variation, moving them towards high-valued solution gradient regions, pulled from neighbouring smooth regions. The floor of the monitor function represents its minimum value: in practice, if first-order derivatives are involved like in (21), the floor is the value of the monitor function when the derivative is zero, so AL monitor is bounded below to unity.

Due to the geometry of our domain, unfortunately, confining layers of the liquid crystal become enriched with grid points, starving the bulk region. Therefore, a monitor function that concentrates a greater amounts of grid points in the core of our domain is desired, with a floor ensuring bounding not necessarily to unity and away from zero: this is done by the BM monitor function introduced by Beckett et al. [29],

$$M(u(z,t)) = \alpha + \sqrt{\left|\frac{\partial u(z,t)}{\partial z}\right|} \tag{22}$$

where

$$\alpha = \int_0^1 \sqrt{\left|\frac{\partial u(z,t)}{\partial z}\right|}\mathrm{d}z. \tag{23}$$

The effect of this floor is to distribute mesh points over the entire domain, thus giving the possibility of more accurate solutions external to boundary regions. It is demonstrated that, with this choice, approximately half of the grid points are located outside the confining layer enabling (22) to cluster more grid points in the core region [29]. In addition, it has the advantage of being self-regulating since the α parameter used to set the floor arises from integration over the entire spatial domain; nevertheless the mesh adaptivity, through α parameter, is controlled at each time step, whereas for AL monitor function, α is a fixed pre-factor of the solution derivative, which is unlikely to hold for the whole calculation; further, a comparison between (21) and (22) shows that the latter is naturally smoothed: for these reasons BM monitor function has the advantage of no need for external interventions.

The solution of our problem modelling leads to a highly non-linear PDE's. We avoid performing error and convergence analysis since it is beyond the scope of the present work. Beckett et al. [29] demonstrate that for one-dimensional problems, the optimal converge rate for dynamical adaptive solutions is achieved using algorithms based on the BM monitor function, rather than the AL monitor function.

The overall adaptive solution process involves two different steps: the generation of a grid and the solution of the PDEs on the grid. In our case, we are interested in solving a multidimensional time-dependent problem and the solution is an iterative process with (1) a mesh generation using the equidistribution principle (based on the numerical solution of current time step) and (2) the solution of the PDEs on the new generated grid and then time updated. In particular we used the following algorithm to solve the MMPDE:

1. a uniform initial grid $z_j[0]$ is generated and the corresponding initial solution $u_j[0]$ is calculated using FEM;
   a temporal loop is done in the time domain updating mesh and solution u, putting forward PDE:
   while $t_n < T$
   the mesh is redistributed in a few steps $\nu \geq 0$:
   do

2. the monitor function is evaluated, the grid is moved from $z_j[\nu]$ to $z_j[\nu+1]$ with an iterative procedure so that to equidistribute the monitor function in each subinterval and a solution $u_j[\nu+1]$ is calculated on the new mesh.

until $\nu \leq \nu_{\max}$

3. the PDE is put forward on the new mesh $z_j[\nu+1]$ to obtain a numerical approximation $u_j[\nu+1]$ at the new time level t_{n+1}.

end

At time $t = 0$ s the grid is uniformly distributed and the solution at the current time is calculated by minimisation of (4) and (12). Steps 2 to 3 and the advance in time of the solution were carried out using the COMSOL Multiphysics finite element package with Matlab [33]. Specifically, at each time step the problem is solved via one step time by minimising the energy density functional, and then the solution u is used to update the monitor function, which equidistribution inside each subinterval moves the mesh point.

4. Order nematic dynamics in a π-cell

Recent works on highly frustrated liquid crystal systems have shown the possibility to induce local transient biaxial order inside a calamitic nematic phase using a mechanical stress or an electric field [7–12]. The π-cell is the main system used to experimentally investigate the biaxial order reconstruction that allows connecting two non-equivalent nematic textures by means of an electric field. The π-cell has sandwich geometry, with a thin film of nematic material confined between two flat glass plates. The internal faces of the glass plates are treated to align the nematic on both surfaces with strong anchoring energy and a pretilt angle θ [34]. The two plates are arranged in an anti-parallel configuration to generate a splay texture [7]. This set-up admits the existence of a second topologically distinct texture where the nematic is π-twisted (or π-bent), and the energy barrier between them, preventing any spontaneous relaxation from each other, gives rise to a topological barrier. The fast switching between these two states is only possible by breaking somewhere the starting nematic texture and reconstructing it with or without the π torsion. In principle this can be achieved by anchoring breaking [35,36] or by melting/reducing the nematic order in a plane [7,37]. In practice, the bulk nematic biaxial order reconstruction induced by the electric field is a mechanism that enables the escape from topological constraints and requires less energy than full melting or anchoring breaking.

The physical problem is modelled with a one-dimensional π-cell of thickness 1 μm with infinite anchoring energy on both plates, when a rectangular electric pulse is applied perpendicular to the boundary plates. As stated above, starting from the splay configuration, the solution of the problem is carried out by an iterative process, which involves at each time step:

1. the generation of the adaptive moving mesh evaluating the monitor function from the previous nematic configuration;
2. the evaluation of the five coupled PDEs, resulting from the Euler-Lagrange equations (4), with the Maxwell equation for the electric potential inside the cell (12), which generates the new nematic configuration for the next time step.

The Euler-Lagrange equations are solved at each time step using a quadratic finite element approximation, whose details can be found in Ref. [12]. In practice, the adaptive mesh is generated by replacing in (21), or in (22) and (23), $u(z,t)$ with $\mathrm{tr}(\mathbf{Q}^2)$. We choose this quantity to monitor the order reconstruction phenomenon because it is the sum of the squared $\mathbf{Q}$ eigenvalues and it varies rapidly in the frustrated region where the degree of order is not constant. The chosen monitor function let to obtain high spatial resolution of the numerical solution inside the cell where the biaxial order reconstruction is expected to occur.

The initial splay configuration has a tilt angle varying almost linearly with z between the boundary values $\theta_L = +10^\circ$ on the lower surface and $\theta_U = -10^\circ$ on the upper surface, where θ is measured with respect to the plate. A fast rectangular pulse electric field, perpendicular to the plates, strong enough to achieve biaxial order reconstruction in the middle of the cell, with amplitude $E = 11.4$ V/μm, is applied at time $t = 1$ ms for a duration of $\tau = 0.25$ ms. The dynamical evolution of the $\mathbf{Q}$ tensor is sampled with a time step size of $\delta t = 0.1$ μs. The numerical simulations were carried out with the typical physical parameters for 5CB nematic liquid crystal at $\Delta T = -2$ °C [38]. In this case, the typical characteristic biaxial coherence length ξ_b is some nanometers and we have discretised the physical domain with a mesh of 285 grid points using the AL and BM monitor functions. In particular, when using an AL monitor function, a further and arbitrary choice for α and number of smoothing loops for the monitor function has to be done: we set $\alpha = 5$ and the number of smoothing loops to 5, which gave the best results. In principle, a larger number of grid points would improve the spatial resolution. In practice, the appropriate number of points is a compromise between spatial resolution and computational effort. Also the nature of the physical problem involved and other external parameters as smoothing loops and, in the case of the AL algorithm, the α parameter settings, can play a significant role in determining the optimal number of points. We have found that, for the problem we treat, 285 grid points give the best compromise. For the sake of completeness, we also performed a computation using the AL algorithm as a benchmark (from now on called the "ALB" algorithm) for the BM algorithm, i.e. setting $\alpha = 0.1689$, which is the last value automatically generated by the BM algorithm, with zero smoothing loops.

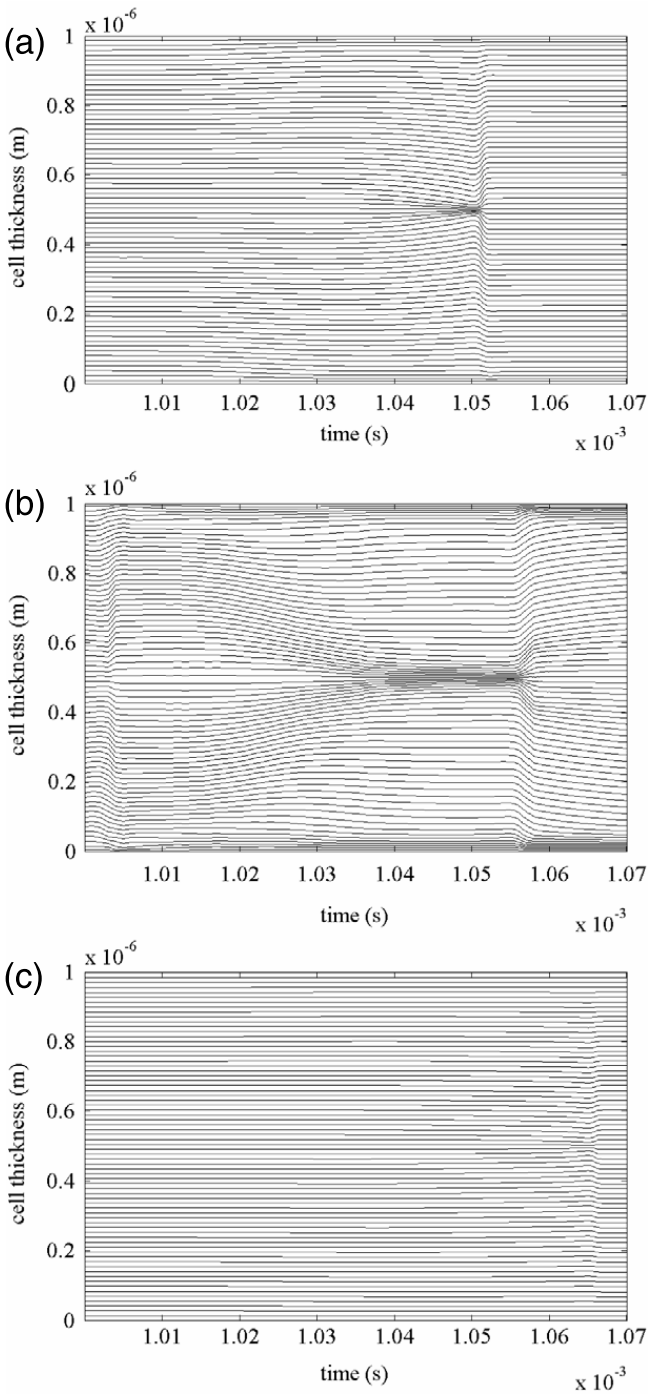

Fig. 1. Node trajectories versus time for AL (a), BM (b) and ALB(c) adaptive mesh algorithms for the time interval 1 ms $\leq t \leq$ 1.07 ms. Only one grid point trajectory in every four has been included. The vertical and the horizontal axis correspond to the z-axis of the nematic π-cell and the time scale of the solution evolution, respectively.

Moreover, to completely characterise the time evolution of the **Q** tensor, we have monitored the biaxiality that arises inside the cell.

5. Numerical results and discussion

Figs. 1 and 2 show the node trajectories for the AL (a), BM (b) and ALB (c) adaptive mesh algorithms for the time interval 1 ms $\leq t \leq$ 1.07 ms, where only one grid point trajectory in every four has been traced. The vertical and the horizontal axis correspond to the cell thickness (z-axis) and the time scale of the solution evolution respectively.

At $t = 0$ s, the initial nematic texture is slightly splayed and in the middle of the cell the director is parallel with the two boundary plates. It remains stable, with no spatial variation of the order tensor **Q**, and the minimisation of (20) results in

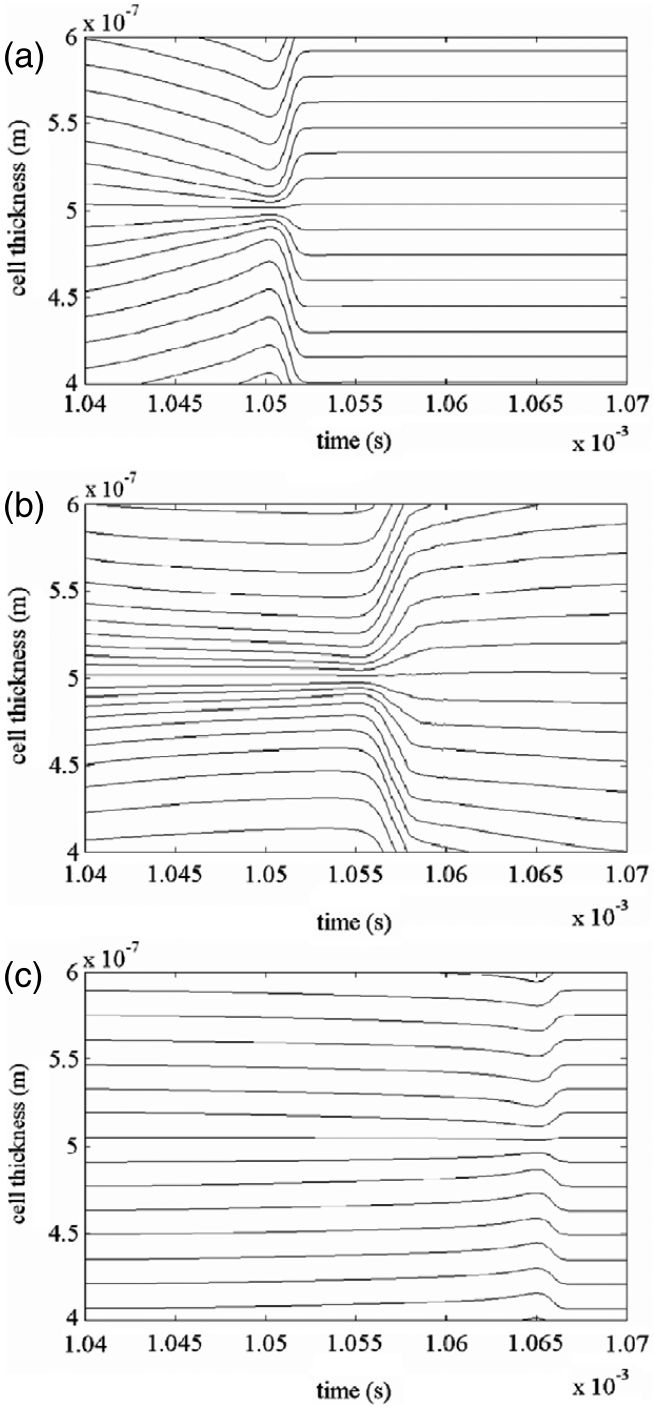

Fig. 2. Magnification of Fig. 1 for AL (a), BM (b) and ALB (c) adaptive mesh algorithms, showing the region around the centre of the cell when the transition from splay to bend occurs.

a uniform distribution of the grid points on the domain. The uniform node trajectories persist until the applications of the electric field.

At time $t = 1$ ms, the electric pulse is applied and the initial splayed nematic texture starts to reorient the nematic molecules along the electric field. The nematic director is almost everywhere perpendicular to the plates, except for three thin regions: the middle of the cell and the two surface layers, where the nematic molecules remain close to their initial orientation. The maximum nematic frustration occurs in the middle of the cell, where a biaxial region of thickness comparable with ξ_b starts to connect the homeotropic upper and lower textures with the middle planar orientation. Fig. 1(a) and (b) show that, as the solution evolves in time, the nodes trajectories moves and they are mainly clustered in the centre of the cell, where the high spatial order variation takes place. In Fig. 1(c), only a faint clustering in the cell's centre is observable, with some time delay with respect to the other two cases. After some tens of microseconds from the application of the

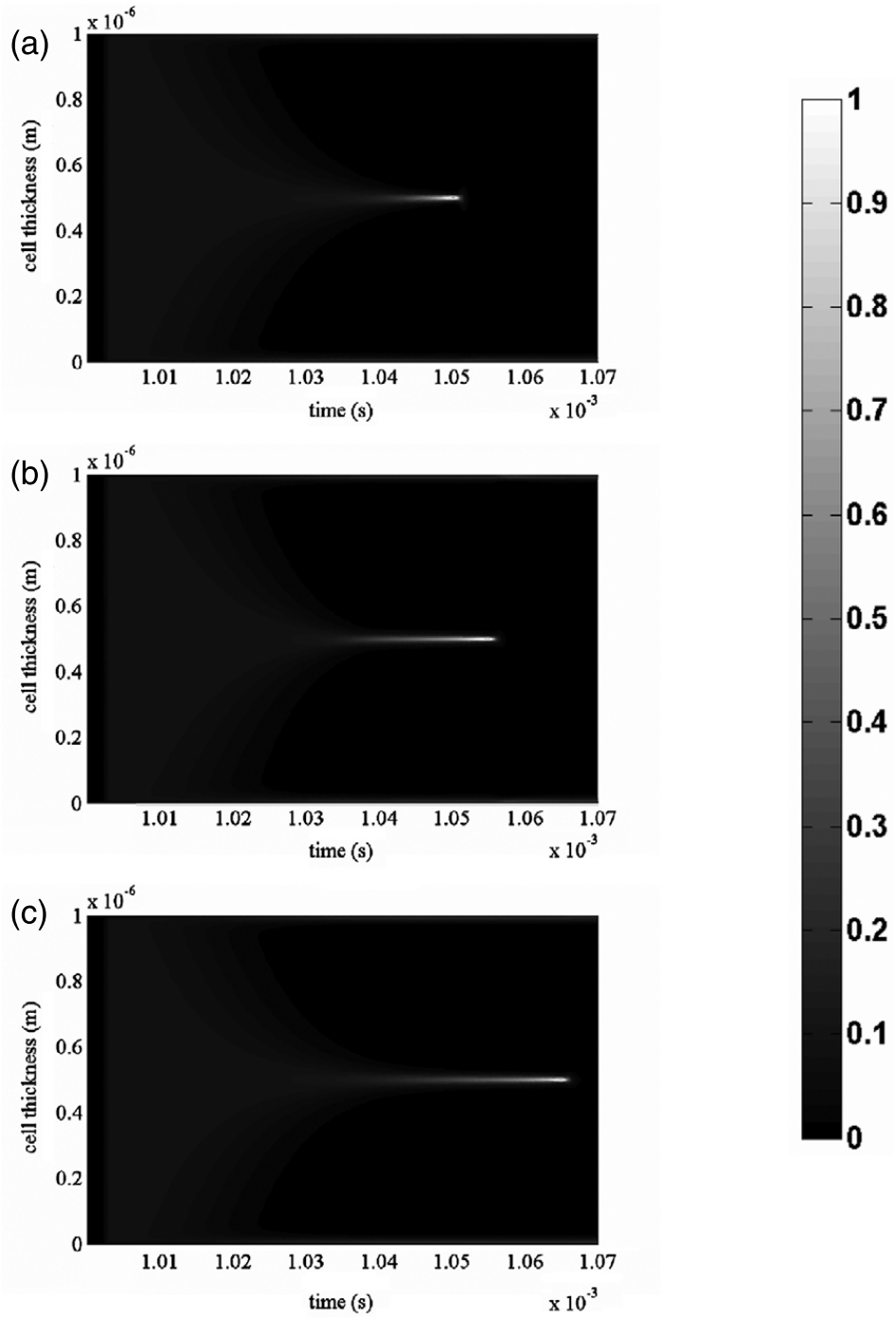

Fig. 3. Surface contour plots of the biaxial order evolution for the 1 ms $\leq t \leq$ 1.07 ms time interval: (a) AL-algorithm; (b) BM-algorithm; (c) ALB-algorithm. The biaxiality is linearly mapped in a grey level scale between black (zero biaxiality) and white (maximum biaxiality) colours.

electric field, the starting splay texture is replaced by a bend texture. The transient bulk biaxial wall allowed the topological barrier connecting the two different nematic textures to be overcome. This phenomenon is completed within 70 μs from the application of the electric field.

Fig. 2 shows a magnification of the node points region around the centre of the cell when the transition from splay to bend nematic texture occurs. After the completion of the splay-bend transition, the nematic order inside the cell is constant and the node points reform a uniform grid.

Comparing the node paths of the AL and BM algorithms (Figs. 1(a), 2(a) and 1(b), 2(b), respectively) with the node path of the ALB algorithm (Figs. 1(c) and 2(c)), it appears that the nematic distortion is better captured by the adaptive grid formed by the AL or BM algorithms, which move the nodes towards the region of large gradient of **Q**, in the middle and in the two surface layers of the cell. Furthermore, at a first insight it seems that the BM monitor function is more efficient to move the node around the nematic distortion: the node grid arising from the BM algorithm (Fig. 1(b) and 2(b)) is denser compared to the other two cases, not only in the central region of the cell, as expected, but also near the confining plates, where a high

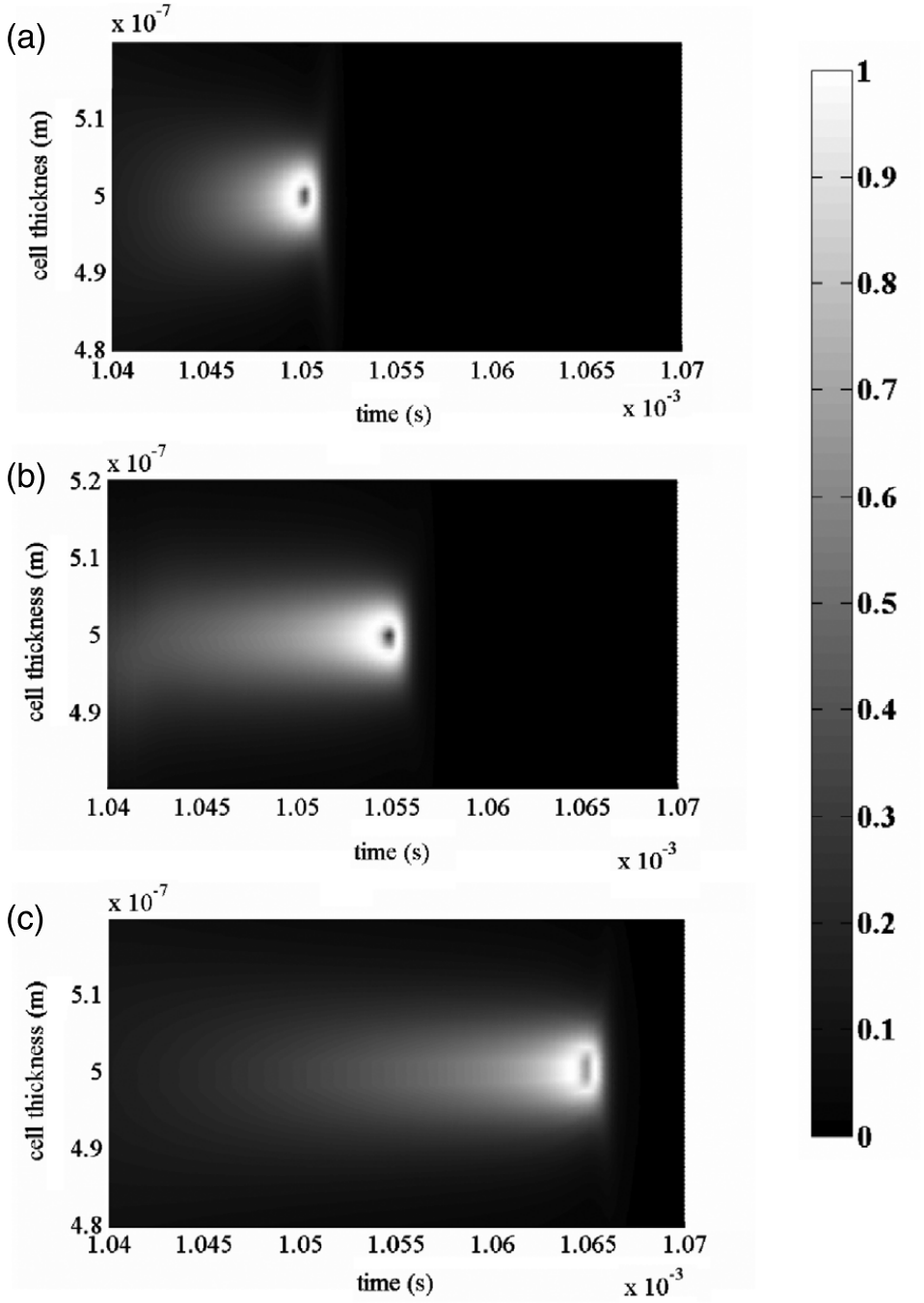

Fig. 4. Magnification of Fig. 3, for AL (a), BM (b) and ALB (c) adaptive mesh algorithms, showing the splay-bend transition mediated by the biaxial wall.

variation of the solution gradient occurs too. A good clustering of grid points in regions where they are necessary allows appreciating smaller variation of the **Q**-tensor.

To better capture the main features of the order reconstruction phenomenon, we evaluated the biaxiality (3) that arises inside the cell during the application of the electric field, which varies between zero for a nematic uniaxial texture and one for a biaxial nematic texture. The biaxial order evolution for the $1\ \text{ms} \leq t \leq 1.07\ \text{ms}$ time interval is shown in Fig. 3, linearly mapped in a grey levels scale between the black (zero biaxiality) and the white (maximum biaxiality) colours. Biaxiality remains zero inside the bulk except for three regions where it is concentrated almost all the nematic distortion. The gradient of the order is a maximum in the middle of the cell: a biaxial region of thickness comparable with ξ_b arises in the bulk and it reaches its maximum in correspondence to the splay-bend transition.

Fig. 4 shows the magnification of the splay-bend transition mediated by the biaxial wall: the maximum of the biaxiality occurs on a ring, while inside it, the biaxiality is zero. After the transition this structure disappears. Fig. 4(a), represents the solution found by the AL algorithm and it is less resolved with respect to Fig. 4(b), obtained via the BM algorithm. In fact, a well-defined dip in the centre of the biaxial ring is clearly observable for the BM case rather than in the AL case. On the

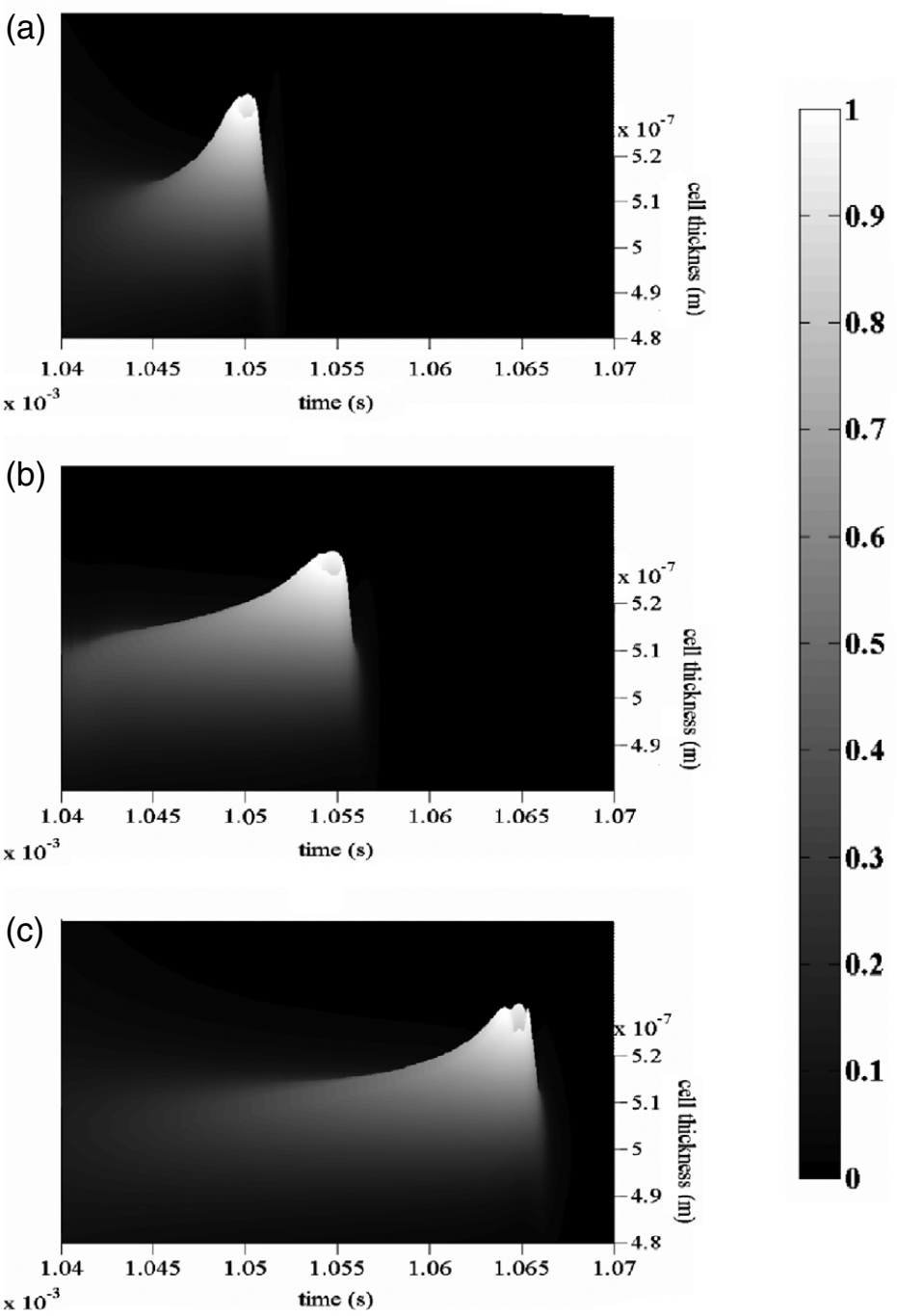

Fig. 5. 3D-plots of surface contour plot of Fig. 4, for AL (a), BM (b) and ALB (c) adaptive mesh algorithms.

other hand, Fig. 4(c) shows the solution obtained by the ALB algorithm: the biaxial region lacks resolution with respect to the other two cases, and the time at which occurs is delayed with respect to the AL and BM results, indicating the poorest convergence feature. Moreover the three-dimensional shape of the biaxiality calculated for the three different adaptive grid mesh algorithms is shown in Fig. 5(a)–(c). The biaxial region looks like a volcano and its crater has a dimension comparable with the biaxial coherence length ξ_b [6,12].

Fig. 6 shows the temporal evolution of the eigenvalues of $\mathbf{Q}$ in the centre of the cell calculated by the AL (a), BM (b) and ALB (c) algorithm. At $t = 0$ s, the largest eigenvalue λ_1, which corresponds to the eigenvector of $\mathbf{Q}$ parallel with the initial horizontal director, decreases as time evolves and is exchanged with λ_3, which corresponds to the eigenvector of $\mathbf{Q}$ in the direction of the field. The maximum biaxiality occurs when λ_1 or λ_3 cross the zero value, while in the dip of the volcano λ_1 and λ_3 are equal and positive and this state corresponds to a planar uniaxial nematic texture with a negative scalar order parameter [15].

Fig. 7 shows the cross-sections of the biaxiality at the cell centre when the splay/bend transition occurs for the three different algorithms. The AL and ALB adaptive mesh grid fail to capture the dip of the volcano crater, while the BM one well

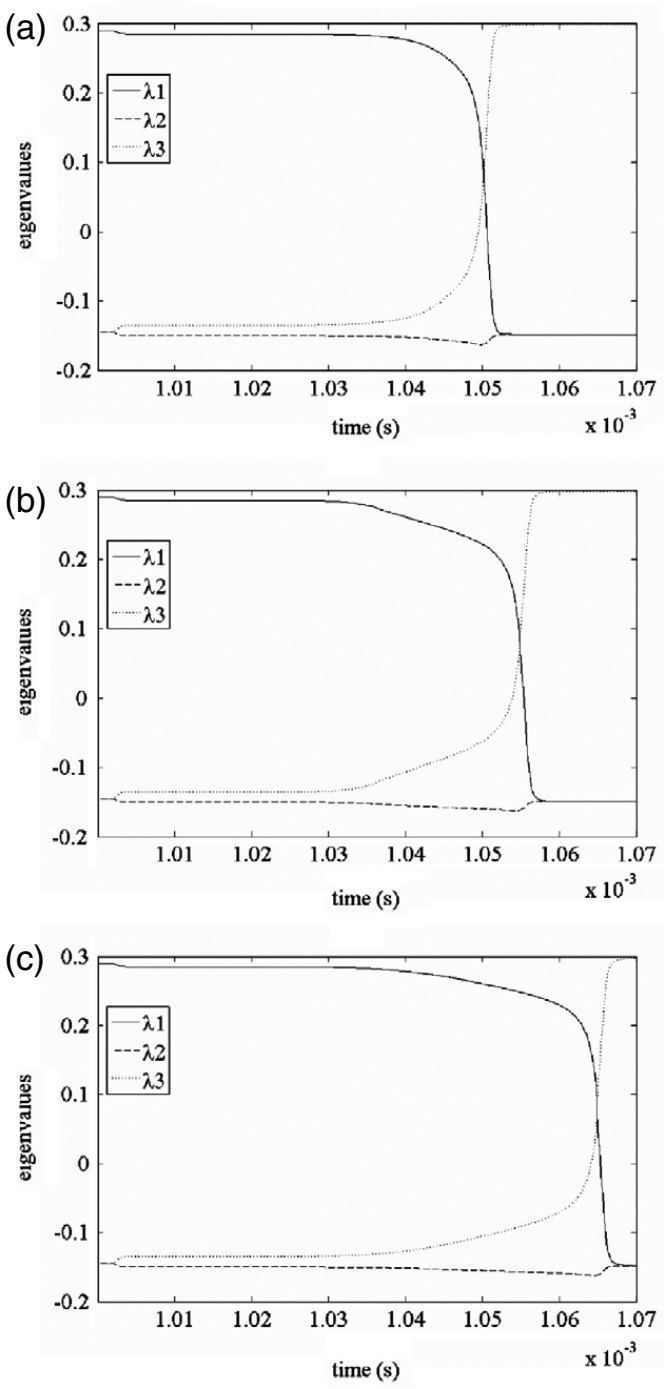

Fig. 6. Plots of the temporal evolution of the **Q** eigenvalues in the centre of the cell calculated by AL (a), BM (b) and ALB (c) algorithms.

represents the structure, with the biaxiality close to zero at the cell centre. The asymmetry of the dip for the AL and ALB mesh grids relative to the cell centre, compared to BM one, indicates that the results obtained with BM monitor function are more reliable than those obtained with the other two methods. In fact, looking at Fig. 2, showing the comparison between meshes arising from the three different algorithms, the meshes arising from the AL algorithm, and especially from the ALB one, are stiffer than those ones arising from the BM algorithm. It follows that the BM algorithm is more adaptive than the AL or ALB algorithms, as it gives more accurate solutions in regions of larger $\nabla\mathbf{Q}$. Moreover the time at which transition occurs is dramatically dependent on an arbitrary choice of the α parameter, as stressed by the comparison between AL and ALB results. Consequently, the AL and ALB are not effective remeshing methods, compared to the BM one, also concerning the absolute time evolution.

Further, in their work Ramage and Newton [25], using a FEM-MMPDE model implemented with an AL monitor function, mimicking the numerical results obtained in Ref. [7] via finite difference discretisation with a uniform grid. Our results, instead, compare directly to those obtained in Ref. [12] using FEM with a *h*-type adaptive grid, in which the starting

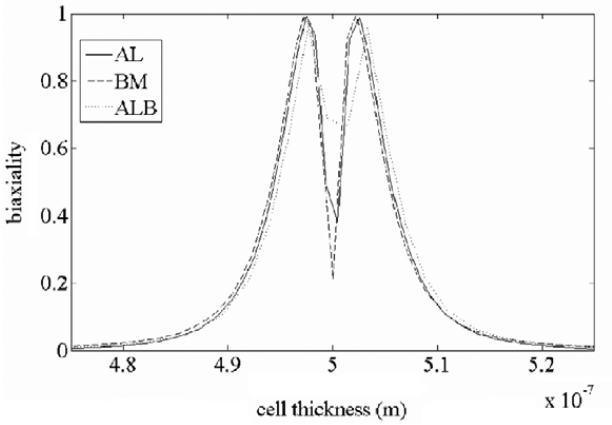

Fig. 7. Cross sections of the biaxiality at the cell centre when the splay to bend transition occurs for AL (a), BM (b) and ALB (c) algorithms.

theoretical model and some physical parameters, as ΔT and electric field amplitude, are different from those used in Refs. [7, 25]. Referring to the pulse start, the biaxial transition time, i.e. the switching time, computed in Ref. [25] is 26 μs early with respect to Ref. [7]; in our case, the switching time obtained via the BM- and AL-algorithm are, respectively, 14 μs and 18 μs early with respect to that computed in Ref. [12]. Although it seems that dynamical remeshing techniques based on gradient of the unknown solution introduce some temporal anticipation with respect to static remeshing techniques, the BM-algorithm gives more accurate results. In addition, we can infer a better effectiveness of the starting theoretical model we use. For the sake of truth, the ALB algorithm gives a switching time which is very near to Ref. [12], but at the expense of the spatial resolution.

6. Conclusions

In this work we implemented a MMPDE finite element method on a dynamical **Q**-tensor model for nematic materials. We started from a Landau-de Gennes model in which the elastic energy density has been expanded up to the third term. Our numerical simulations, never applied before on this model, have been performed using two different monitor functions having different characteristics of mesh points clustering inside the integration domain. Our findings show that the choice of an appropriate monitor function is crucial: the best results, in fact, were obtained by means of the BM monitor function, which does not concentrate mesh points in confining regions of the integration domain, ensuring a more uniform node distribution inside core regions where steep solution variations are located. A consequent resolution improvement of our PDEs model is determined, through appreciable variations of node velocities also occurring in regions of smoother variations of the solution gradient. Once the number of grid points is fixed, this passes through the α-parameter calculation, and in this respect the method has the advantage of being self-regulating. In addition, the BM monitor function is naturally smoothed, having no need of further smoothing loops or, at least, needing a fewer with respect to the AL algorithm. For these reasons, any external arbitrary intervention is avoided or drastically reduced and the assumptions done in Section 2 are confirmed. Accordingly, the use of the BM algorithm instead of the AL one is recommended to solve problems related with nematic order reconstruction phenomena. Work is in progress to extend our model calculations in two dimensions.

References

[1] P.G. de Gennes, J. Prost, The Physics of Liquid Crystals, 2nd ed., Clarendon Press, Oxford, 1993.
[2] C.W. Oseen, Trans. Faraday Soc. 29 (1933) 883.
[3] F. Franck, Discuss. Faraday Soc. 25 (1958) 19.
[4] P. Biscari, P. Cesana, Contin. Mech. Thermodyn. 19 (2007) 285.
[5] N. Schopohl, T.J. Sluckin, Phys. Rev. Lett. 59 (1987) 2582.
[6] G. Carbone, G. Lombardo, R. Barberi, I. Musevic, U. Tkalec, Phys. Rev. Lett. 103 (2009) 167801.
[7] R. Barberi, F. Ciuchi, G. Durand, M. Iovane, D. Sikharulidze, A. Sonnet, E. Virga, Eur. Phys. J. E 13 (2004) 61.
[8] R. Barberi, F. Ciuchi, G. Lombardo, R. Bartolino, G.E. Durand, Phys. Rev. Lett. 93 (2004) 137801.
[9] F. Ciuchi, H. Ayeb, G. Lombardo, R. Barberi, G.E. Durand, Appl. Phys. Lett. 91 (2007) 244104.
[10] H. Ayeb, F. Ciuchi, G. Lombardo, R. Barberi, Mol. Cryst. Liq. Cryst. 481 (2008) 73.
[11] G. Lombardo, H. Ayeb, F. Ciuchi, M.P. De Santo, R. Barberi, R. Bartolino, E.G. Virga, G.E. Durand, Phys. Rev. E 77 (2008) 020702.
[12] G. Lombardo, H. Ayeb, R. Barberi, Phys. Rev. E 77 (2008) 051708.
[13] P. de Gennes, Phys. Lett. 30A (1969) 454.
[14] J. Anderson, P. Watson, P. Bos, LC3D: Liquid Crystal Display 3-D Directory Simulator, Software and Technology Guide, Artech House, Boston, 1999.
[15] E.G. Virga, Variational Theories for Liquid Crystal, Chapman and Hall, London, 1994.
[16] L.V. Mirantsev, E.G. Virga, Phys. Rev. E 76 (2007) 021703.
[17] C. Chiccoli, et al., Phys. Rev. E 67 (2003) 050703.
[18] D. de las Heras, L. Mederos, E. Velasco, Phys. Rev. E 79 (2009) 011712.
[19] O. Zienkiewicz, R. Taylor, The Finite Element Method, Vol. I, Butterworth-Heinemann, Oxford, 2002.
[20] Y. Known, H. Bang, The Finite Element Method Using Matlab, CRC Press, BocaRaon, FL, 2000.

[21] T. Tang, Contemporary Mathematics 383 (2005) 141;
B. Haegland, B. Skaflestad, Preprint numerics no. 2/2002, Norwegian University of Science and Technology, Trondheim, Norway; N. Acikgoz, Ph.D. thesis, Georgia Institute of Technology, USA, 2007.
[22] J.W. Barrett, X. Feng, A. Prohl, Math. Model. Num. Anal. 40 (2006) 175.
[23] P. Patricio, M. Tasinkevych, M.M. Telo da Gama, Eur. Phys. J. E 7 (2002) 117.
[24] R. James, E. Willman, F.A. Fernández, IEEE Trans. Electron Devices 53 (2006) 1575.
[25] A. Ramage, C.J.P. Newton, Liq. Cryst. 34 (2007) 479.
[26] P.D. Brimicombe, E.P. Raynes, Liq. Cryst. 32 (2005) 1273.
[27] M. Ambrožič, F. Bisi, E.G. Virga, Continuum Mech. Thermodyn. 20 (2008) 193.
[28] A. Alexe-Ionescu, Phys. Lett. A 180 (1993) 456.
[29] G. Beckett, J.A. Mackenzie, A. Ramage, D.M. Sloan, J. Comput. Phys. 167 (2001) 372.
[30] C. de Boor, Good approximation by splines with variable knots II, in: Lecture Notes in Mathematics, vol. 363, Springer, Berlin, 1974, pp. 12–20;
V. Pereyra, E.G. Sewell, Numer. Math. 23 (1975) 261;
R.D. Russell, J. Christiansen, SIAM J. Numer. Anal. 15 (1) (1978) 59;
A.B. White, SIAM J. Numer. Anal. 16 (1979) 472.
[31] G. Beckett, J.A. Mackenzie, Appl. Numer. Math. 35 (2000) 87.
[32] W. Huang, J. Comput. Phys. 171 (2001) 753.
[33] COMSOL Multiphysics, http://www.comsol.com/ ; Matlab, http://www.mathworks.com.
[34] A.L. Alexe-Ionescu, R. Barberi, M. Giocondo, G. Cnossen, T.H. van der Donk, Appl. Phys. Lett. 66 (1995) 1701.
[35] G. Barbero, R. Barberi, J. Phys. 44 (1983) 609.
[36] I. Dozov, M. Nobili, G. Durand, Appl. Phys. Lett. 70 (1997) 1179.
[37] P. Martinot-Lagarde, H. Dreyfus-Lambez, I. Dozov, Phys. Rev. E 67 (2003) 051710.
[38] B. Ratna, R. Shashidhar, Mol. Cryst. Liq. Cryst. 42 (1977) 113.